Final Draft
of the original manuscript:

Winzer, N.; Atrens, A.; Dietzel, W.; Song, G.; Kainer, K.U.:
Evaluation of the Delayed Hydride Cracking Mechanism for Transgranular Stress Corrosion Cracking of Magnesium Alloys
In: Materials Science and Engineering A (2007) Elsevier

DOI: 10.1016/j.msea.2007.03.020

Evaluation of the Delayed Hydride Cracking Mechanism for Transgranular Stress Corrosion Cracking of Magnesium Alloys

N. Winzer[a,b], A. Atrens[a,b], W. Dietzel[b], G. Song[a], K.U. Kainer[b]

[a] Materials Engineering, The University of Queensland
Brisbane Australia 4072

a.atrens@minmet.uq.edu.au

[b] Institute for Materials Research, GKSS-Forschungszentrum Geesthacht GmbH,
D-21502 Geesthacht Germany

Abstract

This paper evaluates the important elements of delayed hydride cracking (DHC) for transgranular stress corrosion cracking (TGSCC) of Mg alloys. A DHC model was formulated with the following components: (i) transient H diffusion towards the crack tip driven by stress and H concentration gradients; (ii) hydride precipitation when the H solvus is exceeded; and (iii) crack propagation through the extent of the hydride when it reaches a critical size of ~0.8 μm. The stress corrosion crack velocity, V_c, was calculated from the time for the hydride to reach the critical size. The model was implemented using a finite element script developed in MATLAB. The input parameters were chosen, based on the information available, to determine the highest possible value for V_c. Values for V_c of ~10^{-7} m/s were predicted by this DHC model. These predictions are consistent with measured values for V_c for Mg alloys in distilled water but cannot explain values for V_c of ~10^{-4} m/s measured in other aqueous environments. Insights for understanding Mg TGSCC are drawn. A key outcome is that the assumed initial condition for the DHC models is unlikely to be correct. During steady state stress corrosion crack propagation of Mg in aqueous solutions, a high dynamic hydrogen concentration would be expected to build up immediately behind the crack tip. Stress corrosion crack velocities ~ 10^{-4} m/s, typical for Mg alloys in aqueous solutions, might be predicted using a DHC model for Mg based on the time to reach a critical hydride size in steady state, with a significant residual hydrogen concentration from the previous crack advance step.

1 Introduction

The recent critical review by Winzer et al [i] indicated that TGSCC is the inherent mode of Stress Corrosion Cracking (SCC) for Mg alloys and that the mechanism for TGSCC is still equivocal. It is generally known that TGSCC of Mg involves H [i] and thus TGSCC can be considered an example of Hydrogen Environment Assisted Cracking (HEAC) [ii].

The most recent mechanistic studies [i] have established the important elements in the propagation of TGSCC. Pugh and co-workers [iii, iv, v, vi, vii] proposed that TGSCC occurred by a brittle cleavage mechanism involving H, which resulted in stepped and facetted interlocking fracture surfaces. In contrast, the fractography of Lynch and Trevena [viii] indicated some plasticity, particularly at higher strain rates and crack velocities. Slow strain rate testing by Ebtehaj et al [ix] and Stampella et al [x] suggested a mechanism involving strain induced film rupture leading to corrosion and H production, with crack advance due to H absorption. Makar et al [xi] confirmed the stepped and facetted interlocking fracture surface morphology and the importance of strain rate and H absorption, but proposed a mechanism involving formation and fracture of brittle hydrides. Thus, there is agreement that H is part of the SCC propagation mechanism but disagreement on the role that H plays.

The prior work [i] also indicates that SCC is associated with environmental conditions leading to the local breakdown of a partially protective surface film, allowing absorption of H produced by the Mg corrosion reaction. Film breakdown can be caused by the environment (e.g. pitting due to chloride ions). However, because SCC occurs for: (i) pure Mg in a dilute sulphate solution; and (ii) Mg alloys (AZ91, AM60, AS41, ZK60A-T5) in distilled water indicates that film breakdown may also be a role of the mechanical loading.

Important characteristics of TGSCC of Mg alloys that must be rationalised by any TGSCC mechanism include: (i) that the stress corrosion crack velocity, V_c, has been measured by Speidel [xii] to be independent of the applied stress intensity factor, K_1, and by Pugh et al [xiii] to be proportional to K_1^2 above a critical stress intensity factor for SCC, K_{ISCC}; (ii) that crack propagation is discontinuous (as evidenced by discrete

high-amplitude acoustic emissions [xiv, xv, xvi, xvii, xviii]); (iii) the development of a stepped and interlocking fracture surface [xv, xix, xx, xxi]; (iv) that the fracture process zone, l_{fpz}, is typically 0.1 – 0.8 μm (as evidenced by parallel markings within cleavage steps associated with consecutive crack arrest fronts [xiv, xv, xvi, xvii]), and (v) that measured values for K_{ISCC} lie the range 4 – 14 MPa.m$^{1/2}$ [xii,xxii].

The most likely mechanism for TGSCC of Mg alloys is Delayed Hydride Cracking (DHC) [i, xiv, xvi, xix, xxiii]. Previous workers have proposed various models relevant to DHC in hydride-forming metals, particularly Zr alloys. Liu [xxiv] and van Leeuwen [xxv] derived analytical solutions for the steady state and transient distribution, respectively, of lattice H ahead of a sharp crack; however, these models did not include hydride precipitation. Dutton et al [xxvi] derived an expression for the rate of hydride growth in the elastic field ahead of a crack tip in Zr by assuming: (i) a steady state flux through the crack tip; and (ii) that the hydride grows in line with the crack with a uniform thickness of twice the crack tip radius. More recent models [xxvii, xxviii, xxix, xxx, xxxi] used finite element analysis (FEA) solutions to the diffusion equations. The FEA approach has not previously been applied to DHC in Mg alloys. The FEA method facilitates consideration of the influence of hydride precipitation on H diffusion and stress distribution. These FEA models assumed isotropic conditions (except for that proposed by Varias and Massih [xxix]) and considered the interrelation of diffusion/precipitation and lattice deformation.

This paper provides a critical evaluation of the DHC mechanism in TGSCC of Mg alloys. A numerical DHC model was formulated for the TGSCC of Mg alloys. This model was implemented using a FEA script developed in MATLAB. The DHC model was used to predict values for V_c for comparison with experimental measurements (as summarised in the next section). The DHC model was critically evaluated to determine the maximum predicted values for V_c.

2 Crack Velocities for TGSCC in Mg

Values for V_c reported by various workers for TGSCC in Mg are summarised in Table 1. Table 1 indicates a wide range of values for V_c depending on the test conditions.

For example, Ebtehaj et al [xxii] and Makar et al [xxiii] measured a broad range of V_c values ($8x10^{-8}$ - $2x10^{-5}$ m/s) by varying the environmental composition and the applied stress or stress intensity factor. Similarly, Speidel [xii] measured $V_c = 3x10^{-9}$ to $8x10^{-9}$ m/s for ZK50 in distilled water, $V_c = 1x10^{-5}$ m/s in 5m NaBr and $V_c = 6x10^{-4}$ m/s in 1.4m Na_2SO_4. The fastest stress corrosion cracking velocities (~10^{-4} m/s) are attributed to unimpeded hydrogen ingress at the crack tip. Slower stress corrosion crack velocities could be due to hydrogen ingress impedance, such as due to a partially-protective surface film. Lynch and Trevena's [xxxiv] measured values for V_c (as high as $5x10^{-2}$ m/s) were significantly higher than the other researchers. Their high V_c values were produced by cantilever bend tests at high deflection rates, and may have incorporated some ductile tearing.

The V_c values given in Table 1 correspond to a wide range of measurement techniques, all of which are widely accepted. This may contribute to the spread in data:

- Bursle and Pugh [xiv] calculated V_c from measured distances between consecutive parallel steps on the fracture surface and the time intervals between corresponding acoustic emissions.
- Pugh et al [xiii] and Speidel et al [xii] measured V_c directly using travelling microscopes. The two techniques used by Pugh and co-workers [xiii, xiv] gave consistent V_c values.
- Wearmouth et al [xxi] measured the crack length by stopping the test at various time intervals.
- Makar et al [xxiii] divided the length of fracture surface corresponding to SCC by the test duration.
- Winzer et al [xxxii] measured similar stress corrosion crack velocities for AZ91 in distilled water using SSRT and LIST [xxxiii].

Material	Environment	Load Conditions	Crack Velocity [m/s]	Reference
Mg-7.5Al	NaCl+K_2CrO_4	-	$3x10^{-5}$	xiv
Mg-7.6Al	NaCl+K_2CrO_4	Constant load	$6x10^{-6}$ - $4x10^{-5}$	xiii
Mg-7Al	NaCl+K_2CrO_4	SSRT	$2x10^{-6}$ - $5x10^{-6}$	xxi
ZK50A-T5	Distilled H_20	Constant load	$3x10^{-9}$ - $8x10^{-9}$	xii
ZK50A-T5	1.4m Na_2SO_4	Constant load	$6x10^{-4}$	xii
ZK50A-T5	5m NaBr	Constant load	10^{-5}	xii
Mg-7.6Al	NaCl+K_2CrO_4	Constant load	10^{-5}	xvii
Mg-8.8Al	NaCl+K_2CrO_4	SSRT	10^{-7} - $8x10^{-6}$	xxii
Mg-8.8Al	NaCl+K_2CrO_4	Constant load	$2x10^{-6}$ - $3x10^{-5}$	xxii
Mg-8.8Al	NaCl+K_2CrO_4	Constant strain	$8x10^{-7}$ - $2x10^{-5}$	xxii
RSP Mg-1Al	NaCl+K_2CrO_4	SSRT	$2x10^{-7}$ - 10^{-5}	xxiii
RSP Mg-9Al	NaCl+K_2CrO_4	SSRT	$8x10^{-8}$ - $3x10^{-6}$	xxiii
Pure Mg	NaCl+K_2CrO_4	Const deflection rate	10^{-8} - $5x10^{-2}$	xxxiv
AZ91	Distilled water	SSRT	$7x10^{-10}$ - $5x10^{-9}$	xxxii
AZ91	Distilled water	LIST	$5x10^{-9}$	xxxii

Table 1 – Measured stress corrosion crack velocities for Mg alloys.

3 The DHC Mechanism for TGSCC in Mg

3.1 Overview of Issues

This section evaluates the important elements of the DHC mechanism for Mg TGSCC, particularly with respect to determining V_c. Prediction of V_c requires identifying and modelling the rate-limited process. DHC involves repeated stages of: (i) H-ingress; (ii) diffusion of H ahead of the crack tip (driven by chemical potential and H-concentration gradients); (iii) hydride formation when the H concentration exceeds the local solvus (which is dependent on the crack tip stress field); and (iv) fracture of the brittle hydride. Furthermore, hydride precipitation is accompanied by deformation of the adjacent lattice due to the dissimilar atomic volumes of the hydride and the Mg metal. The deformation is coupled with precipitation because the resulting change in the stress field decreases the force driving diffusion of lattice H. These issues are reviewed in the following subsections.

3.2 H Ingress

Corrosion of Mg [xxxv, xxxvi, xxxvii, xxxviii, xxxix, xl] involves the partial reactions given by Equations 1 and 3. Production of H occurs by the cathodic partial reaction given by Equation 3. Cathodically-produced monatomic H resides at the metal surface for some time before combining into H_2 gas [xli]. This time allows some H atoms to be absorbed into solid solution, where they are partly dissociated into a proton and electron [xli, xlii, xliii, xliv, xlv, xlvi] (Equation 4).

$$Me \rightarrow Me^{n+} + ne^- \qquad 1$$

$$H^+_{aqu} \rightarrow H^+_{ads} \qquad 2$$

$$H^+_{ads} + e^-_{metal} \rightarrow H_{ads} \qquad 3$$

$$H_{ads} \rightarrow H_{metal} \text{ where } H_{metal} = H^+_{metal} + e^-_{metal} \qquad 4$$

The remaining adsorbed H-atoms recombine (by Equation 5) to produce gaseous H_2, which is partly soluble in water. H_2 bubbles are produced when the solution is locally saturated with H [xlii, xliii].

$$H_{ads} + H_{ads} \rightarrow H_2 \qquad 5$$

Crolet and Bonis [xliii] proposed that a H^+ ion in the aqueous solutions might transfer directly (by Equation 6) into the metal solid solution without undergoing reduction and dissociation.

$$H^+_{aqu} \rightarrow H^+_{metal} \qquad 6$$

H ingress may be a rate-limiting factor for HEAC in gaseous H because dissociation of H_2 molecules is necessary and H ingress may be inhibited by surface films [xli]. In contrast, H ingress is expected not to be a rate-limiting factor in TGSCC of Mg, which is generally associated with exposure to an aqueous environment, when H evolution and entry occurs at bare metal surfaces exposed by active corrosion or mechanical rupture of the surface film [i, xxxv, xxxvi].

3.3 Hydrogen Diffusion

H-diffusion in an isothermal material is driven by chemical potential and concentration gradients. Chemical potential is partly defined by stress. The principal stresses for a sharp crack tip in a linear-elastic isotropic material are:

$$\sigma_{xx} = \frac{K_1}{\sqrt{2\pi r}} \cos\left(\frac{\theta}{2}\right)\left[1 - \sin\left(\frac{\theta}{2}\right)\sin\left(\frac{3\theta}{2}\right)\right] \qquad 7a$$

$$\sigma_{yy} = \frac{K_1}{\sqrt{2\pi r}}\cos\left(\frac{\theta}{2}\right)\left[1+\sin\left(\frac{\theta}{2}\right)\sin\left(\frac{3\theta}{2}\right)\right] \qquad 7b$$

$$\sigma_{z} = v\left(\sigma_{xx}+\sigma_{yy}\right) \qquad 7c$$

where K_I is the crack tip stress intensity factor and θ is the angle relative to the crack plane. Thus, the hydrostatic stress field, σ_{kk}, is characterised by:

$$\sigma_{kk} = \frac{1}{3}\sum\sigma_{ii} = \frac{2(1+v)K_1}{3\sqrt{2\pi r}}\cos\left(\frac{\theta}{2}\right) \qquad 8$$

where v is Poisson's ratio. The influence of crack tip plasticity is neglected in the present work (see Section 3.8).

The fluxes due to stress and concentration gradients are additional [xxiv, xlvii]. Because the solute and solvent atoms have different sizes, the oversized solute atoms cause strain in the surrounding lattice and thus interact with hydrostatic stress fields [xlvii]. This interaction acts as a driving force for oversized solute atoms to move towards a tensile crack tip. Fick's first law states that for an isothermal system the diffusion flux through any plane in the absence of stress is proportional to the concentration gradient:

$$J = -D\nabla C \qquad 9$$

where C is the concentration of the solute atoms in the lattice and D is the coefficient of diffusion. The force acting on the solute atom due to an external stress only is equal to the chemical potential gradients, ∇U . The resulting flux is given by:

$$J = -\frac{DC}{kT}\nabla U \qquad 10$$

where k is Boltzman's constant and T is temperature in Kelvin. D/kT is the mobility of the solute atom. The total flux due to concentration and stress gradients is given by summing Equations 9 and 10:

$$J = -D\left(\nabla C + \frac{C}{kT}\nabla U\right) \qquad 11$$

It follows that the differential equation for the distribution of solute H is:

$$\frac{dC}{dt} = D\nabla\left(\nabla C + \frac{C}{kT}\nabla U\right) \qquad 12$$

If the solute atom is considered a sphere and its corresponding interstice an undersized hole then U can be approximated by:

$$U = -\frac{1}{3}\sigma_{kk}\bar{V}_H \qquad 13$$

where $\bar{V}_H$ is the partial molar volume of H in solid solution or change in volume of the spherical hole. It may be important to note that Equation 13 neglects the strain energy due to accommodation of the H atom as given by Dutton et al [xxvi]. $\bar{V}_H$ may be approximated from the radii of the solute and solvent atoms as per Liu [xxiv]:

$$\bar{V}_H = 4\pi\gamma_0^3\frac{\gamma - \gamma_0}{\gamma_0} \qquad 14$$

where γ and γ_0 are the radii of the solute and solvent atoms respectively. The $\bar{V}_H$ value of $7\text{x}10^{-7}\text{m}^3$/mol used by Varias and Massih for Zr is reasonably valid for Mg since Mg and Zr have approximately equal atomic radii (150 pm and 155 pm respectively).

3.4 Hydrogen Diffusion Coefficient

An issue for previously proposed mechanisms for TGSCC of Mg involving H diffusion was the apparent low value (~$1\text{x}10^{-12}$ m^2/s) for the hydrogen diffusion coefficient, which was obtained by extrapolation of high-temperature data to room temperature. The low value was difficult to correlate with measured values for V_c using any mechanism based on H diffusion [xxxiv]. More recent data extrapolated to room temperature indicate a much higher value for the diffusion coefficient for H in Mg ($1\text{x}10^{-9}$ m^2/s) [xlviii]. This value has been used in the present investigation.

3.5 Influence of Stress on Solvus Concentration

Puls [xlix] proposed that, in the absence of external stress, the solvus concentration, c_{con}, for H in the metal lattice in equilibrium with a metal hydride of composition MH_a in a constrained matrix differs from the solvus concentration in a stress-free environment, c_s, according to the relationship:

$$c_{con} = c_s \exp\left(\frac{\overline{W}_{acc}}{aRT}\right) \qquad 15$$

where $\overline{W}_{acc}$ is the total molar strain energy of the matrix and hydride resulting from the volumetric misfit and is given by [l, li]:

$$\overline{W}_{acc} = -\frac{1}{2}\int_V \sigma_{ij}^I \varepsilon_{ij}^T dV \qquad 16$$

where V is the volume of the hydride, σ_{ij}^{I} is the stress in the hydride, ε_{ij}^{T} is the strain in the matrix resulting from transformation of volume, V, from metal, M, to hydride, MH_a. A simplified solution for $\overline{W}_{acc}$ may be derived by idealising the hydride as a spherical inclusion in a cavity with a lesser unstrained radius such that expansion of the surrounding matrix is uniform [l, lii]:

$$\overline{W}_{acc} = 6G\delta^2 V \Big/ \left(1 + \frac{4G}{3K}\right) \qquad 17$$

where V is the initial volume of the cavity, K is the bulk modulus of the hydride, G is the shear modulus of the matrix and δ is the normalised difference between the unstrained radii of the hydride and cavity. If the number of moles of metal in the hydride and the lattice displaced by the cavity are equal, then δ may be calculated according to [liii]:

$$\frac{\Omega_{hr}}{\Omega_m} = (1+\delta)^3 \qquad 18$$

where Ω_{hr} and Ω_m are the molar volumes of the hydride and metal. If ε is the radial expansion of the cavity, then the corresponding compression of the hydride is $\delta - \varepsilon$ such that the hydrostatic stress within the hydride is [liii]:

$$\sigma_h = 3K(\delta - \varepsilon) \qquad 19$$

Mott and Nabarro [liii] showed that δ and ε are related by:

$$\varepsilon = \delta\left(1 - \frac{3K}{3K + 2E/(1+\nu)}\right) \qquad 20$$

where and E and ν are the Young's Modulus and Poisson's ratio for the matrix respectively. In the present case for Mg, Ω_{hr} was calculated to be 18.56×10^{-6} m^3/mol from the X-ray density of MgH_2 given by Ellinger et al [liv]. K is taken as 49 GPa [lv]. The well-known values for Ω_m, E and ν are 14×10^{-6} m^3/mol, 44 GPa and 0.35 respectively [lvi]. From these values it is possible to calculate from Equations 18 and 20 that for a spherical MgH_2 inclusion $\varepsilon = 0.03$ independent of the hydride radius.

The solvus concentration is further influenced by external stress according to the relationship [xlix, xxix]:

$$c_s^{\sigma} = c_s \exp\left(\frac{\bar{W}_{acc} + \bar{W}_{\text{int}}}{aRT}\right)\exp\left(\frac{\sigma_{kk}\bar{V}_H}{RT}\right) \qquad 21$$

where $\overline{W}_{int}$ is the interaction between the external stress field and transformation strain respectively, given by [lii]:

$$\overline{W}_{\text{int}} = -\int_V \sigma_{ij}^e \varepsilon_{ij}^T dV \qquad 22$$

where σ_{ij}^e is the local stress due to the externally applied loads. Lufrano [xxvii] proposed that in the presence of a highly concentrated and variable stress field, such as that near a crack tip, Equation 22 can be expressed explicitly as:

$$\overline{W}_{\text{int}} = -\frac{\sigma_{kk}}{3(1-b)}\left(V_{hr} - \left(\overline{V}_M + b\overline{V}_H\right)\right) \qquad 23$$

where b is the ratio of hydrogen to metal atoms in solid solution and V_{hr} and V_M are the molar volume of the hydride and partial molar volume of the metal in solid solution respectively.

3.6 Solvus Concentration

Krozer and Kasemo [lix] measured that the solvus concentration for H in Mg in the absence of external stress is approximately 2 at. % at 353 K. This value was based on permeation experiments using low-pressure gaseous H_2 and Pd-coated Mg membranes at close-to ambient temperature. Thus, it was assumed that this value includes the influence of $\overline{W}_{acc}$. Moreover, in the region ahead of the crack tip (where there is high stress according to Equation 8) $\overline{W}_{acc} << \overline{W}_{\text{int}}$ for hydrides < 1 mm in diameter; that is, the strain energy due to the volumetric misfit is negligible compared to the interaction between the concentrated stress field and the transformation strain. Therefore, in the context of stress-directed diffusion of H towards a crack tip, the H solvus concentration is dependent only on the applied stress field, and Equation 21 may be reduced to:

$$c_s^{\sigma} = c_{con} \exp\left(\frac{\overline{W}_{\text{int}}}{aRT}\right)\exp\left(\frac{\sigma_{kk}\bar{V}_H}{RT}\right) \qquad 24$$

Figure 1 shows the normalised concentration c_s^{σ}/c_{con} in the region ahead of the crack tip for various applied K_1 values near K_{1SCC}. A reduction in the solvus concentration

of several orders of magnitude immediately ahead of the crack tip is apparent. It should be recalled that $\overline{W}_{int}$, and therefore c_s^{σ}/c_{con}, is dependent on b (the ratio of hydrogen to metal atoms in solid solution) according to Equation 23. In Figure 1, b is furnished by the equilibrium solvus concentration along the crack line, which is given by [xxiv]:

$$c = c_0 \exp\left(-\frac{U}{kT}\right) \qquad 25$$

where c_0 is the concentration at the crack surface and U is given by Equation 8 and Equation 13 for $\theta = 0$.

An alternative evaluation of the H solvus in Mg is as follows. The solubility of hydrogen in metals obeys Sievert's law, which is given by:

$$c_s = K_S f_H^{1/2} \qquad 26$$

where C_S is the solubility (given as an atomic fraction), K_s is the solubility constant and f_H is the equilibrium H fugacity, which at low values is approximately equal to the gas pressure. Nishimura et al [lvii] determined experimentally (in the temperature range 200 to 220°C) that K_s is given by:

$$K_S = 1.8 \times 10^{-1} \exp\left(\frac{-1.16 \times 10^4}{RT}\right) \qquad 27$$

where K_s is in units of mol H_2 m^{-3} $Pa^{-1/2}$. Figure 2 plots the solvus concentration of H in Mg (in terms of the equilibrium hydrogen pressure, P_H) against 1000/T as reported by previous workers [lviii, lix, lx]. The trend line through the data has the expression:

$$P_H = 1.149 \times 10^7 \exp\left(\frac{-9 \times 10^3}{T}\right). \qquad 28$$

Figure 2 also plots the vapour pressure of Mg [lxi] for comparison. The H solvus concentration (as an atomic fraction) can be evaluated by combining Equations 26 - 28, assuming that the hydrogen pressure is a good approximation for the hydrogen fugacity. This gives the following equation:

$$c_s = 2.698 \exp\left(\frac{-5.897 \times 10^3}{T}\right) \qquad 29$$

Equation 29 is plotted in Figure 3. This equation for the H solvus in Mg is consistent with that in Zr [lxii]. The corresponding H solvus in magnesium at 293 K is 4.9×10^{-9}. This is in stark contrast to the measurements of Krozer and Kasemo [lix] (also plotted

in Figure 3). Both approaches appear credible, so there needs to be experimental research to determine the actual H solvus in Mg, particularly at temperatures relevant to TGSCC of Mg. In the absence of an experimental resolution of this issue, the modeling in this paper has been carried out separately using both values for the H solvus concentration.

It is also worth noting that the hydrogen atomic fraction 4.9×10^{-9} corresponds to a hydrogen concentration of 2×10^{20} atoms/m^3. This is a useful reference number with respect to the hydrogen concentrations used in the modeling in Section 5.

3.7 Influence of Hydride Accommodation on Stress Field

The volume expansion of the lattice to accommodate hydride formation serves to relax tensile stresses near the crack tip. This section evaluates the magnitude of this effect to determine the consequences of neglecting the influence of hydride accommodation on the stress field with respect to the prediction of V_c.

The influence of hydride accommodation on the stress field may be approximated by idealizing the hydride as an oversized spherical inclusion of radius r_0 embedded in an infinite matrix as per Section 3.5. With the origin of the coordinate system at the interface of the hydride and matrix, the strains in the matrix are given by [liii]:

$$\phi_{xx} = -2\varepsilon\left(\frac{r_0}{r}\right)^3 \qquad 30$$

$$\phi_{yy} = \varepsilon\left(\frac{r_0}{r}\right)^3 \qquad 31$$

$$\phi_{zz} = \phi_{yy} \qquad 32$$

where ε is given by Equation 20 and r is the distance from the centre of the hydride. Hooke's law gives:

$$-2\varepsilon E\left(\frac{r_0}{r}\right)^3 = \sigma_{xx} - 2\nu\sigma_{yy} \qquad 33$$

$$\varepsilon E\left(\frac{r_0}{r}\right)^3 = -\nu\sigma_{xx} + (1-\nu)\sigma_{yy} \qquad 34$$

$$\sigma_{zz} = \sigma_{yy} \qquad 35$$

where σ_{xx}, σ_{yy} and σ_{zz} are the corresponding stresses and E is the elastic modulus of the matrix. Given that ε = 0.03 (as determine in Section 3.5) the accommodation stress may be determined for any given r_0. Figure 4 shows that the accommodation stress (calculated as a von Mises stress) in the matrix adjacent to the hydride is severe, and that plastic deformation would result.

With some iteration it can also be shown that the hydrostatic stress in the matrix due to hydride accommodation only is given by:

$$\sigma_{kk}^{hyd} = \frac{4}{3}\varepsilon E\left(\frac{r_0}{r}\right)^3 \qquad 36$$

Equation 36 is equivalent to the expression given by Liu [xxiv] for the chemical potential of the H atom in solid solution (see Equations 13 and 14). Thus σ_{kk}^{hyd} at the hydride matrix interface (i.e. where $r = r_0$) is independent of the size of the hydride.

Figure 5 shows the hydrostatic accommodation stress, σ_{kk}^{hyd}, for a hydride of radius 0.5 μm and the hydrostatic stress, σ_{kk}, ahead of a sharp crack tip (calculated according to Equation 8) for various K_1 values. For K_1 = 6 MPa.m$^{1/2}$ (which corresponds to reported values of K_{1SCC} [xii, xxii]) σ_{kk}^{hyd} is small relative to σ_{kk} and can be ignored. However, for lower values of K_1 (<1 MPa.m$^{1/2}$) σ_{kk}^{hyd} may exceed σ_{kk} near the metal-hydride interface. The crack tip stress field and the accommodation stress are opposite in sign. Thus, for low K_1 values σ_{kk}^{hyd} can overwhelm σ_{kk} near the metal-hydride interface, thus nullifying or reversing the chemical potential gradient and therefore the H flux (according to Equation 11). This may explain the existence of a critical K_1 value, K_{1SCC}, below which TGSCC does not occur. An expression for K_{1SCC} may be given in terms of the critical hydride radius, r_{crit}, by combining Equations 8 and 35 for $r = r_0$ (i.e. at the hydride-matrix interface):

$$K_{1SCC} = \frac{\varepsilon E\sqrt{8\pi r_{crit}}}{(1+\nu)} \qquad 37$$

r_{crit} may be approximated from the fracture process zone, l_{fpz}. The range of values for K_{1SCC} corresponding to the reported values for l_{fpz} (0.1 - 0.8 μm [xiv, xv, xvi, xvii]) is 1.5 - 4.4 MPa.m$^{1/2}$. This is consistent with lower values for K_{1SCC} given by previous workers (4 – 14 MPa.m$^{1/2}$) [xii, xxii].

A DHC model that neglects the influence of the hydride accommodation on the applied stress field would differ from that described by Sofronis and co-workers [xxvii, xxviii]. Moreover, the complexity of the model is significantly reduced. Maintaining a time-constant stress field during the FEA modeling process (for example, as defined by Equation 8) eliminates the necessity to resolve the influence of hydride accommodation on the stress field for consecutive stages of hydride growth. Furthermore, since the volume expansion of the lattice to accommodate hydride formation serves to relax tensile stresses near the crack tip, this simplification somewhat exaggerates the chemical potential gradients that partially drive diffusion of solute H and, consequently, the hydride growth rate.

3.8 The Influence of Crack Tip Plasticity

Previous models for DHC (particularly in Zr) [xxvi, xxviii, xxx] have assumed a K_I-mode stress distribution at the crack tip as per Equation 8. Some justification may be derived from the fracture topography of TGSCC for Mg; the fracture surfaces indicate a brittle fracture process and generally do not indicate localised plasticity [i, xxxii]. However, for values of K_I of the same magnitude as K_{ISCC}, the influence of plasticity and the crack tip plastic zone on H-diffusion ahead of the crack tip could be significant. An approximation for the radius of the plastic zone at a crack tip is given by [lxiii]:

$$r_{pz} = \frac{b}{2\pi}\left(\frac{K_I}{\sigma_y}\right)^2 \qquad 37$$

where b = 1 for plane stress and $b = (1\text{-}2\nu)^2$ for plane strain. For $K_I = K_{ISCC}$ (~6 MPa.m$^{1/2}$ [xii, xxii]) and typical mechanical properties values for Mg-alloys (ν = 0.35 and σ_Y = 110 MPa), Equation 37 predicts that r_{pz} = 40 μm for plane strain conditions. This is considerably larger than the fracture process zone ($l_{fpz} \approx$ 0.1-0.8 μm [xiv, xv, xvi, xvii]). Stress in the plastic zone is considered relatively uniform and equal to ~3σ_Y [ii]. Therefore, according to Equation 11 the driving force for diffusion within the plastic zone would be dominated by the concentration gradient, and would be considerably less than for a K_I mode stress field. The approach adopted in the present work has been to determine the highest value for Vc, which would correspond to the

highest driving force for diffusion. Hence, a K_I-mode stress field as has assumed as has been done by previous workers [xxvi, xxviii, xxx].

3.9 Hydride Fracture Criteria

Shi and co-workers [lxiii, lxiv] proposed that hydride fracture occurs when the local stress inside the hydride, σ_l, exceeds some critical stress, which is a mechanical property of the hydride. σ_l is the sum of the intra-hydride stress due to the precipitation process only, σ_h, and the stress normal to the crack due to external loads, $\sigma_\perp$. These stresses are opposite in sign; σ_h is compressive and $\sigma_\perp$ is tensile.

In the fully elastic case, $\sigma_\perp$ can be evaluated Equation 7. Since σ_h is a uniform hydrostatic stress (given by Equation 19) and is independent of the hydride radius, it is difficult to understand how hydride fracture could occur at some critical hydride size. The same conclusion is drawn for the case of hydride fracture within the plastic zone.

It may be important to note that, since hydride accommodation is plastic, Equation 19 would over-estimate σ_h; it would not be unreasonable to expect less plastic accommodation for small hydrides, thus increasing their resistance to fracture.

Previous research has reported fine parallel markings approximately 0.1 - 0.8 μm apart within cleavage planes on SCC fracture surfaces [xiv, xv, xvi]. These markings were interpreted as corresponding to consecutive stages of crack advance. Therefore, a plausible model can assume that fracture occurs when the hydride reaches a critical size of 0.1 - 0.8 μm ahead of the crack tip. In the present work, a critical hydride size of 0.8 μm was assumed.

3.10 Proposed DHC Model

Based on the above evaluation, a DHC model is proposed based on transient hydrogen diffusion towards and, when the H solvus concentration is exceeded, hydride precipitation in the region ahead of the crack tip. The model evaluates V_c based on the time-to-reach the critical hydride dimension during stage-2 crack growth. The model has been solved for the two literature values for the H solvus

concentration: (i) 0.02 and (ii) 4.9 x 10^{-9}. H ingress is assumed through either: (i) the whole crack surface or (ii) a distance around the crack tip comparable to the crack tip opening displacement.

4 FEA Formulation of the DHC Model

A finite element script was developed in MATLAB to solve for the transient H distribution and hydride precipitation ahead of a sharp crack tip. The concept for this program is presented as a flow diagram in Figure 6.

4.1 Initial and Boundary Conditions and Mesh Considerations

H diffusion and hydride precipitation in the elastic stress field was simulated for a 3 x 1.5 μm region at the crack tip. This region was discretised using 900 uniform linear triangular elements. Since the K_I stress field (defined by Equation 8) is symmetrical about the crack plane, its origin was placed at the bottom of the mesh as close as possible to the crack tip as was allowed by the program, as shown in Figure 7. A small, arbitrary and uniform H concentration, c_0, (typically $0 < c_0 \leq 10^5$ atoms/m^3) was applied to the mesh at the beginning of each simulation and maintained at the crack surface for all time. Flux was enabled at the crack surface and calculated using Equation 11 for the average concentration, concentration gradient and chemical potential gradient at each element along the crack surface. Flux at other boundaries including that ahead of the crack tip was disabled.

4.2 The Finite Element Equations

The finite element equations for transient diffusion of solute H due to concentration and stress gradients can been derived by applying the method of weighted residuals to Equation 12. For a two-dimensional elastic solid [xxiv]:

$$\nabla^2\left(\sigma_{xx}+\sigma_{yy}\right)=0 \qquad 39$$

Consequently, Equation 12 can be reduced to:

$$\frac{dC}{dt}=D\nabla^2 C+\frac{D}{kT}\nabla C\nabla U \qquad 40$$

The integral for the weight residual statement for Equation 40 is:

$$I = \int_{\Omega} D\nabla^2 C d\Omega - \int_{\Omega} w \frac{D}{kT} \nabla C \nabla U d\Omega + \int_{\Omega} w \frac{\partial C}{\partial t} d\Omega \qquad 41$$

The governing differential equation is given by the weak formulation for the integral of the weighted residual statement, which is given by applying Green's Theorem to Equation 41 [xxix, xxx, xxxi]:

$$\int_{\Gamma} w \frac{\partial C}{\partial n} d\Gamma = \int_{\Omega} D\left(\frac{\partial w}{\partial x} \frac{\partial C}{\partial x} + \frac{\partial w}{\partial y} \frac{\partial C}{\partial y} \right) d\Omega - \int_{\Omega} w \frac{D}{kT} \nabla C \nabla U d\Omega + \int_{\Omega} w \frac{\partial C}{\partial t} d\Omega \qquad 42$$

where Γ and Ω are the bounding surface and area of the domain and w denotes the typical weighting functions (in this case defined by the shape functions for linear triangular elements).

Equation 42 is more conveniently expressed in matrix form [xxvii, xxviii]:

$$\{F\} = [M]\{\dot{C}\} + [K]\{C\} \qquad 43a$$

where

$$[M] = \int_{V} [A]^T [A] dV \qquad 43b$$

$$[K] = [K_1] + [K_2] \qquad 43c$$

$$[K_1] = \int_{V} [B]^T D [B] dV \qquad 43d$$

$$[K_2] = \int_{V} [B]^T \frac{D\bar{V}_H}{3kT} [B] \{\sigma_{kk}\} [A] dV \qquad 43e$$

$$\{F\} = -\int_{S} [A]^T \mathbf{J} dS \qquad 43f$$

Where $\{C\}$ and $\{\sigma_{kk}\}$ are the nodal concentration and hydrostatic stress vectors respectively, $[A]$ and $[B]$ are the standard time-independent interpolation matrices for transient diffusion problems and **J** is the component of the flux normal to the bounding surface S. $[K]$ and $[M]$ are the so-called diffusivity and concentration matrices respectively. In this case $[K]$ is separated into components corresponding to the first and second terms in Equation 12, $[K_1]$ and $[K_2]$ respectively. The vector $\{F\}$ contains the flux at the crack surface given by Equation 11.

4.3 Iterative Procedure

The forward and reverse difference methods were found to be unstable for iterating Equation 43, whereas solution was possible using the modified reverse difference method proposed by Sofronis et al [xxviii]. Substituting Equation 43c into 43a for time $t+\Delta t$ gives:

$$[M]\{\dot{C}\}_{t+\Delta t} + [K_1]\{C\}_{t+\Delta t} = \{F\} - [K_2]\{C\}_{t+\Delta t} \qquad 44$$

Sofronis et al assumed that for each iteration $\{F\}$-$[K_2]\{C\}$ can be take from the previous step:

$$\left(\{F\} - [K_2]\{C\}\right)_{t+\Delta t} = \left(\{F\} - [K_2]\{C\}\right)_t \qquad 45$$

The conventional reverse difference method assumes that $\{\dot{C}\}$ may be approximated by:

$$\{\dot{C}\}_{t+\Delta t} = \frac{\{C\}_{t+\Delta t} - \{C\}_t}{\Delta t} \qquad 46$$

Combining Equations 44 to 46 gives:

$$\left[\frac{1}{\Delta t}[M] + [K_1]\right]\{C\}_{t+\Delta t} = \frac{1}{\Delta t}[M]\{C\}_t + \{F\}_t - [K_2]\{C\}_t \qquad 47$$

It should be recalled that $[K_1]$ and $[K_2]$ vary for each iterative step due to their dependence on D. Similarly, [M] varies for each iterative step due its dependence on the hydride concentration (see below). Consequently, in order to calculate $\{C\}_{t+\Delta t}$ it was necessary to assume that for each iteration [M], $[K_1]$ and $[K_2]$ could be taken from the previous step.

Equation 47 was solved for $\{C\}_{t+\Delta t}$ for a number of time increments until the hydride size was ~ 0.8 μm (the assumed values for l_{fpz}) ahead of the crack tip. Hydride precipitation was characterised by the hydride volume fraction, f, as per Sofronis and co-workers [xxvii, xxviii]. The nodal values of f were linearly interpolated between f = 0 when H exists only in solid solution and f = 1 when the lattice material has been converted entirely to hydride:

$$f = \begin{cases} 0 & \text{if} \quad c < c_s^\sigma \\ \dfrac{c - c_s^\sigma}{c_h - c_s^\sigma} & \text{if } c_s^\sigma \le c < c_h \\ 1 & \text{if} \quad c_h \le c \end{cases} \qquad 48$$

where c is the molar equivalent of C and c_h is the concentration at which the entire lattice becomes hydride. c_h is given by the molar concentration of H in MgH_2, which is 0.66.

Transformation of the lattice from metal to hydride is associated with a reduction in D (and the amount of H remaining in solution) of several orders of magnitude [lix, lxv]. Consequently, it was necessary re-calculate the elemental matrices constituting [M], [K_1] and [K_2] according to the variation in f in the corresponding elements for each iterative step. It was assumed that D could be interpolated linearly such that $D = 10^{-9}$ m^2/s when $f = 0$ and $D = 0$ when $f = 1$. The value of D (required for Equations 43d and 43e) was calculated for each element by averaging the values for the 3 connected nodes. The elemental matrices could be adjusted for each iteration according to:

$$[M]^e_{t+\Delta t} = \left(1 - [f]^e_t\right)[M]^e_t \qquad 49a$$

$$[K_1]^e_{t+\Delta t} = \left(1 - [f]^e_t\right)[K_1]^e_t \qquad 49b$$

$$[K_2]^e_{t+\Delta t} = \left(1 - [f]^e_t\right)[K_2]^e_t \qquad 49c$$

where [f] is a diagonal matrix containing the nodal values of f for each element.

5 DHC Model Predictions

5.1 Hydride Distribution

A typical result for the DHC model is presented in Figure 8. It shows contours of equal values of f. The region bounded by $f = 1$ is comprised completely of hydride, whereas at the next contour, $f = 0.95$, there is 95 % hydride and 5 % Mg metal. In this case, DHC was simulated for $K_1 = K_{1SCC} \approx 6$ MPa.$m^{1/2}$, neglecting the influence of the plastic zone, for a period of time corresponding to $f = 1$ at a distance of ~0.8 µm ahead of the crack tip. The initial H concentration in the region near the crack tip (and subsequent concentration at the crack surface) was zero. A small, arbitrary H concentration and flux (calculated according to Equation 11) was maintained at the crack surface. The hydride nucleated at the point of maximum hydrostatic stress and the growth of the hydride followed the hydrostatic stress distribution.

For most of the simulation time (~4.5 sec) $f < 0$ for the entire domain; the greatest period of time (t ~ 4.5 sec) is that which is required for c to reach c_s^{σ} at the point of maximum stress, then hydride first forms and thereafter the hydride grows rapidly. Figure 9 shows the hydride distribution for various times between (i) complete hydride throughout the first element (when $c = c_h$ at the point of maximum stress) and (ii) when the $f = 1$ front is 0.8 μm ahead of the crack tip (assuming $K_1 = 6$ MPa/m$^{1/2}$). The time corresponding to $f = 1$ at 0.8 μm ahead of the crack tip is $t \approx 6.2$ sec. Assuming that the crack propagates through the $f = 1$ zone only, this corresponds to $V_c = 1.3 \times 10^{-7}$ m/s. This idealization assumes that there is no possibility of crack arrest at some discontinuity in the hydride. However, it should be noted that crack propagation may be possible wherever $f > 0$, which accounts for a significant region further ahead of the $f = 1$ front.

These predictions for V_c are dependent on initial conditions that are somewhat variable, particularly K_1 and the H concentration at the crack surface, C_{surf}. The sensitivity of the DHC model to these parameters was investigated as follows.

5.2 Influence of H Solvus

V_c was also calculated for $c_s = 4.9 \times 10^{-9}$ (the value obtained by extrapolation of existing data to room temperature). The time taken for the $f = 1$ front to reach 0.8 μm ahead of the crack tip (assuming $K_1 = 6$ MPa/m$^{1/2}$ and a crack surface concentration of 10^5 atom/m^3) was ~5.6 sec. This corresponds to $V_c = 1.4 \times 10^{-7}$ m/s. The time required for the H concentration to reach the solvus at the point of maximum stress (~2.9 sec) was less than for $c_s = 0.02$ (~4.5 sec); however, a greater period of time was required for the hydride to develop (i.e. $0 < f \leq 1$) due to the greater difference between c_s and c_h (~2.7 sec). Consequently, given the assumed fracture criteria, c_s has a minimal effect on V_c.

5.3 Influence of K_1

Figure 10 shows the influence of K_1 near K_{1SCC} (1 MPa.m$^{1/2}$ to 20 MPa.m$^{1/2}$) on the time required for the $f = 1$ hydride front to reach a distance of ~0.8 μm ahead of the crack tip for $D = 1 \times 10^{-9}$ m^2/s in a 3 x 1.5 μm region around the crack tip. The calculated values are reasonably log-linear. The deviation from the log-linear trend

line was attributed to the decreasing accuracy of the program as K_1 tends towards 10 MPa.m$^{1/2}$. The trend line has the expression:

$$t = 7.6 \times 10^3 K_1^{-0.45} \qquad 50$$

If the critical hydride size is constant for all values of K_1 (which is true only if the fracture process zone is smaller than r_{pz}), it follows that:

$$V_C \propto K_1^{2.2} \qquad 51$$

This is relatively consistent with reports by Pugh, Green & Slattery [xiii] that $V_C \propto K_1^2$ for Mg-7.6Al in NaCl-K_2CrO_4 solution. A similar relationship was reported by Speidel et al [xii] for ZK50A alloy in distilled water, but not Na_2SO_4 or NaBr solutions. It may be important to remember that this correlation relies on the critical hydride size being constant for all values of K_1, which may not be true even in the elastic stress field. Hydride fracture occurs when the intra-hydride stress, which the sum of $\sigma_\perp$ and σ_h, exceed some critical stress, which is a mechanical property of the hydride (see Section 2.9) [lxiii, lxiv]. Consequently, since σ_h is dependent on the hydride geometry only, in the elastic stress field the critical hydride size must be dependent on K_1, although the specific nature of this dependency is not known.

Liu [xxiv] proposed that the relationship $V_C \propto K_1^2$ could also be explained by assuming that the rate limiting process for DHC was the reaction to produce MgH_2; if Vc is proportional to the reaction rate (or H concentration) then $V_C \propto K_1^2$ if $K_1 \propto \sqrt{a}$, where a is the critical hydride size.

5.4 Location of H Ingress

The model assumes that the H flux (given by Equation 11) through the crack surface is unimpaired by protective films. This assumption is reasonable given that the assumed crack surface is only ~1.5μm in length. However, it is important to note that the extent of the crack surface for which H absorption may occur is dependent on the inherent rate of repassivation and the environmental conditions at the crack tip, and that for a given stress distribution and crack surface concentration, V_c does decrease as the crack surface available for H ingress is reduced (for K_1 = 6 MPa/m$^{1/2}$, a 40% reduction in crack surface area results in a 25% reduction in V_c).

5.5 H Concentration at the Crack Surface

Figure 11 shows the influence of the H concentration at the crack surface, C_{surf}, on the time, t, to reach the critical hydride size for $K_I = K_{ISCC} \approx 6$ MPa.m$^{1/2}$ and $D = 10^{-9}$ m^2/s. t is inversely proportional to log(C_{surf}) for $C_{surf} > 0$ atoms/m^3 (if $C_{surf} = 0$ there is no flux though the crack surface according to Equation 11). If the critical hydride size is constant for all values of K_I, then V_c is also proportional to log(C_{surf}). This suggests that C_{surf} is a significant factor in determining V_c. Consequently, there exists a need to determine the actual surface concentration by experimental measurements. It also indicates that V_c is relatively insensitive to small changes in C_{surf}. This is contrary to the experimental results of Speidel [xii] that suggest that V_c is highly dependent on H concentration at the crack surface. Speidel [xii] measured $V_c = 3\text{x}10^{-9}$ to $8\text{x}10^{-9}$ m/s for ZK50 in distilled water, $V_c = 1\text{x}10^{-5}$ m/s in 5m NaBr and $V_c = 6\text{x}10^{-4}$ m/s in 1.4m Na_2SO_4.

The dashed line in Figure 11 shows the influence of C_{surf} on t when the flux through the crack surface is dependent on the stress gradient only (i.e. the first term in Equation 11 is ignored). The two lines are generally similar, although there is considerable deviation for low values of C_{surf}. This suggests that V_c is primarily dependent on the stress gradient at the crack surface for most values of C_{surf}. This may explain the low-sensitivity of V_c to variations in C_{surf}.

Figure 11 also shows that t approaches zero as C_{surf} approaches $9\text{x}10^{26}$ atoms/m^3, which corresponds with the solvus concentration in the absence of stress as given by Krozer and Kasemo [lix]. Since the hydrostatic stress at the crack surface is zero (according to Equation 8), an impermeable hydride layer develops at the crack surface when C_{surf} exceeds this value, preventing H diffusing ahead of the crack tip and causing hydride formation.

6 Comparison with Literature

Assuming a critical hydride size of 0.8 µm for all values of K_I, the values predicted by the present DHC model for V_c as shown in Figure 10 and Figure 11 range from $4.6\text{x}10^{-8}$ m/s to $3.3\text{x}10^{-7}$ m/s. These DHC model predictions are consistent with the

lower measured crack velocities reported by previous workers, as summarised in Table 1 and thus could explain the stress corrosion crack velocity for Mg alloys in distilled water. However, the DHC model as presently formulated does not predict stress corrosion crack velocity values of 10^{-5} m/s as measured e.g. by Speidel [xii] for the stress corrosion cracking of ZK50 in dilute NaBr solution or by Pugh and co-workers [iii, iv, v, vi, vii] for Mg-Al alloys in NaCl + K_2CrO_4.

7 Discussion

The DHC model had the following components: (i) transient H diffusion towards the crack tip driven by stress and H concentration gradients; (ii) hydride precipitation when the H solvus is exceeded; and (iii) crack propagation through the extent of the hydride when it reaches a critical size of ~0.8 μm. The stress corrosion crack velocity, V_c, was calculated from the time for the hydride to reach the critical size.

The DHC model and input parameters were consistent with the prior literature [xxvii, xxviii, xxix, xxx, xxxi]. Most of the input parameters used in the model have been carefully selected based on the information available [xxix, lvi, lviii, lix, lx]. However, some parameters that have considerable influence on V_c are somewhat speculative as discussed in Section 3. They include: (i) the diffusion coefficient for H in Mg and MgH_2; (ii) the critical hydride size; (iii) the H solvus concentration in the absence of stress; and (iv) the partial molar volume of H in Mg. These were selected to determine the highest possible value for V_c.

The model is critically based on a hydrostatic stress distribution near the crack tip defined by a time-independent K_I-mode stress distribution (given by Equation 8). It is difficult to characterise the stress field at a crack tip at the scale defined by the assumed l_{fpz} (i.e. <1 μm) due to in homogeneities in the material. However, the K_I-mode stress distribution has been used for DHC models [xxv, xxvii, xxix] and results in the highest possible driving force for H-diffusion.

Alternative mechanisms for TGSCC of Mg alloys involving hydride formation may cause higher crack velocities than DHC are: (i) hydride dislocation locking (HDL) or

(ii) film rupture. HDL [lxvi] involves preferential segregation of hydrogen at dislocation cores in the region ahead of the crack tip. Hydrides precipitate when there is a sufficient local hydrogen concentration. A relatively small hydrogen concentration is postulated to cause embrittlement by locking the dislocations in place and preventing their motion. This HDL model requires a local crack-tip hydrogen concentration much lower than that of the DHC model, and would thereby predict crack velocity values higher than predicted by the DHC model. The film rupture model was proposed by Pugh et al [13]. This might involve brittle crack initiation due to a brittle oxide or hydride followed by crack propagates some distance into the ductile matrix.

It was also assumed that the crack propagates through the extent of the region where the metal had been entirely converted to hydride (i.e. where $f = 1$) when the $f = 1$ front reached the critical size. This idealisation is difficult to rationalise, as the hydride distribution ahead of the crack tip is unlikely to be homogeneous and crack propagation is possible further ahead of the $f = 1$ front (i.e. wherever $0 < f \leq 1$).

A key outcome is that the standard initial condition for DHC models is unlikely to be correct. It was assumed that the region near the crack tip was free of H and that H diffuses from the crack surface only. This assumption, although made in previous DHC models [xxvi, xxvii, xxix], is valid only for the initial crack propagation step in a "virgin" H-free material and not steady state propagation. In the case of the initial crack propagation in a "virgin" H-free material it is appropriate to choose a low, uniform H concentration as an initial condition. This is depicted in Figures 8 and 9. For steady state propagation the appropriate hydrogen concentration around the crack tip can be deduced from Figure 8 by moving the point of origin to the right by a distance corresponding to the prior crack advance (~0.8 μm), such that the new crack tip is in a region with a hydride volume fracture $f = 0.95$ rather than a hydrogen concentration of ~ 0. Figure 9 shows that in an "annealed" material the growth of the region corresponding to $f = 1$ grew to ~0.8 μm in 0.02 s. Given an initial condition of $f = 0.95$ at the crack tip, the predicted crack velocity is then:

$$V_c = 0.8\ \mu m/0.02\ s = 4 \times 10^{-5}\ m/s. \qquad 52$$

This estimation shows that the DHC model may be developed to predict a crack velocity is sufficiently high to explain the stress corrosion crack velocities in Table 1 measured by Speidel [xii], Pugh et al [xiii], Ebtehaj et al [ix] and Makar et al [xi].

8 Conclusions

- Some critical input parameters for the DHC model are not known with adequate precision, particularly at ambient temperatures. These include: (i) the hydrogen diffusion coefficient for H in the Mg lattice and in MgH_2; (ii) the H solvus in magnesium; (iii) the critical hydride size; and (iv) the partial molar volume of H in Mg.
- K_{1SCC} may be defined by the interaction between the hydride accommodation stress an the crack tip stress field such that for $K_1 < K_{1SCC}$ there is insufficient driving force for hydrogen to be attracted to the crack tip.
- The DHC model predicts similar values of *Vc* for: (i) a wide range of H solvus concentrations (as given by the literature); and (ii) H concentration at the various distances along the crack flank.
- The DHC model predicts that $V_C \propto K_1^2$, which is consistent with reports by Pugh, Green & Slattery [xiii] for Mg-7.6Al in NaCl-K_2CrO_4 solution.
- Stress corrosion crack velocities ~10^{-4} m/s, which are typical for Mg alloys in aqueous solutions, cannot be predicted by the DHC model based on the time to reach a critical hydride size for material with a low initial H concentration throughout. Such velocities might be predicted by a DHC model based on the time to reach the critical hydride size in steady state, when a significant hydrogen concentration would have built up at the crack tip.
- During steady state stress corrosion crack propagation of Mg in aqueous solutions, a high dynamic hydrogen concentration would be expected to build up just behind the crack tip. This may be a feature of all cases of SCC where the crack propagation mechanism is HEAC.

9 Acknowledgements

The authors wish to thank the GM Technical Centre at Warren MI, the Australian Research Council (ARC), the Australian Research Network for Advanced Materials (ARNAM) and GKSS-Forschungszentrum Geesthacht GmbH. M Pfuff is thanked for frank useful frank discussions.

10 References

i Winzer N., Atrens A., Song G., Ghali E., Dietzel W., Kainer K.U., Hort N., Blawert C.: A Critical Review of the Stress Corrosion Cracking (SCC) of Magnesium Alloys, Adv. Eng. Mater., 7, No. 8, 2005, pp659-693

ii RP Gangloff, Hydrogen-assisted cracking, in *Comprehensive structural integrity*, I Milne, RO Ritchie and B Karihaloo eds, *Vol 6 Environmentally assisted failure*, (2003) 31-101.

iii A.J. Bursle, E.N. Pugh, in *Mechanisms of Environment Sensitive Cracking of Materials*, ed P.R. Swann, F.P. Ford and A.R.C. Westwood, Materials Society (London), 1977, 471

iv D.G. Chakrapani, E.N. Pugh, *Metallurgical Transactions* 1975, *6A,* 1155

v D.G. Chakrapani, E.N. Pugh, *Corrosion* 1975, *31,* 247

vi D.G. Chakrapani, E.N. Pugh, *Metallurgical Transactions* 1976, *7A,* 173

vii E.H. Pugh, J.A.S. Green, P.W. Slattery, *Fracture 1969: The Proceedings of the Second International Conference on Fracture*, ed P.L. Pratt, Chapman and Hall Ltd, London 1969, 387

viii S.P. Lynch, P. Trevena, *Corrosion* 1988, *44,* 113

ix K. Ebtehaj, D. Hardie, R.N. Parkins, *Corrosion Science* 1993, *28,* 811

x R.S. Stampella, R.P.M. Procter, V. Ashworth, *Corrosion Science* 1984, *24,* 325

xi G.L. Makar, J. Kruger, K. Sieradzki, *Corrosion Science* 1993, *34,* 1311

xii Speidel M.O., Blackburn M.J., Beck T.R., Feeney J.A.: Corrosion Fatigue and Stress Corrosion Crack Growth in High Strength Aluminium Alloys, Magnesium Alloys and Titanium Alloys Exposed to Aqueous Solutions, Corrosion Fatigue: Chemistry, Mechanics and Microstructure, NACE-2, 1972, pp324-345

xiii E.H. Pugh, J.A.S. Green, P.W. Slattery, "On the Propagation of Stress-Corrosion Cracks in a Magnesium-Aluminium Alloy", *Fracture 1969: The Proceedings of the Second International Conference on Fracture*, ed P.L. Pratt, Chapman and Hall Ltd, London (1969) 387

xiv A.J. Bursle, E.N. Pugh, "On the Mechanism of Transgranular Stress-Corrosion Cracking", in *Mechanisms of Environment Sensitive Cracking of Materials*, ed P.R. Swann, F.P. Ford and A.R.C. Westwood, Materials Society (London), (1977) 471-481

xv D.G. Chakrapani, E.N. Pugh, "On the Fractography of Transgranular Stress Corrosion Failures in a Mg-Al Alloy", *Corrosion* 31 (1975) 247-252

xvi D.G. Chakrapani, E.N. Pugh, "Hydrogen Embrittlement in a Mg-Al Alloy" *Metallurgical Transactions* 7A (1976) 173-178

xvii D.G. Chakrapani, E.N. Pugh, "The Transgranular SCC of a Mg-Al Alloy: Crystalographic, Fractographic and Acoustic-Emission Studies", in *Metallurgical Transactions* 6A (1975) 1155-1163

xviii W.M. Pardue, F.H. Beck, M.G. Fontana, "Propagation of Stress-Corrosion Cracking in a Magnesium-Base Alloy as Determined by Several Techniques" *Transactions of the American Society for Metals*, 54 (1961) 539-548

xix EI Meletis, RF Hochman, "Crystallography of Stress Corrosion Cracking in Pure Magnesium", *Corrosion* 40 (1984) 39-45

xx RS Stampella, RPM Proctor, V Ashworth, "Environmentally Induced Cracking of Magnesium", *Corrosion Science* 24 No 4 (1984) 325-341

xxi WR Wearmouth, GP Dean, RN Parkins, "Role of Stress in the Stress Corrosion Cracking of a Mg-Al Alloy", *Corrosion* Vol. 29 No. 6 NACE 1979 251-258

xxii K. Ebtehaj, D. Hardie, R.N. Parkins, "The Influence of Chloride-Chromate Solution Composition on the Stress Corrosion Cracking of a Mg-Al Alloy" *Corrosion Science* 28 (1993) 811-829

xxiii GL Makar, J Kruger, K Sieradzki, "Stress Corrosion Cracking of Rapidly Solidified Magnesium-Aluminium Alloys", *Corrosion Science* 34 No. 8, 1311-1342, 1993

xxiv H.W. Liu, "Stress-Corrosion Cracking and the Interaction Between Crack-Tip Stress Field and Solute Atoms", *Transactions of the ASME*: Journal of Basic Engineering, 1970, Vol 92, p633-638.

xxv H.P. Van Leeuwen, "The Kinetics of Hydrogen Embrittlement: A Quantitative Diffusion Model", Engineering Fracture Mechanics, Vol 6, pp141-161, 1974

xxvi R. Dutton, K. Nuttall, M.P. Puls, L.A. Simpson, "Mechanisms of Hydrogen Induced Delayed Cracking in Hydride Forming Materials", *Metallurgical Transactions* 8A, pp1553-1562, 1977

xxvii J Lufrano, P Sofronis, HK Birnbaum, "Modelling of Hydrogen Transport of Elastically Accommodated Hydride Formation Near a Crack Tip", *J. Mech. Phys. Solids*, Vol 44, No 2, 179-205, 1996

xxviii P. Sofronis, R.M. McMeeking, "Numerical Analysis of Hydrogen Transport Near a Blunting Crack Tip", *J. Mech. Phys. Solids*, Vol 37, No 3, pp317-350, 1989

xxix A.G. Varias, A.R. Massih, "Hydride-Induced Embrittlement and Fracture in Metals – Effect of Stress and Temperature Distribution", *J. Mech. Phys. Solids*, Vol 50, pp1469-1510, 2002

xxx A.G. Varias, J.L. Feng, "Simulation of Hydride Induced Steady-State Crack Growth in Metals – Part I: Growth Near Hydrogen Chemical Equilibrium", Computational Mechanics, Vol 34, pp339-356, 2004

xxxi A.G. Varias, J.L. Feng, "Simulation of Hydride Induced Steady-State Crack Growth in Metals – Part II: General Near Tip Field", Computational Mechanics, Vol 34, pp357-376, 2004

xxxii N Winzer, G Song, A Atrens, W Dietzel and KU Kainer, Stress Corrosion Cracking of Mg, Invited Keynote Paper, *3rd International Conference on Environmental Degradation of Engineering Materials*, May 2007, Gdansk Poland.

xxxiii A Atrens, CC Brosnan, S Ramamurthy, A Oehlert and IO Smith. Linearly Increasing Stress Test (LIST) for SCC Research, *Measurement Science and Technology*, 4 (1993) 1281-1292

xxxiv SP Lynch, P Trevena, "Stress Corrosion Cracking and Liquid Metal Embrittlement in Pure Magnesium", *Corrosion* 44, 113-124, 1988

xxxv G Song and A Atrens, Corrosion Mechanisms of Magnesium Alloys, *Advanced Engineering Materials* 1 (1999) 11-33.

xxxvi GL Song and A Atrens (Invited Review) Understanding Magnesium Corrosion Mechanism: a Framework for Improved Alloy Performance, *Advanced Engineering Materials* 5 (2003) 837

xxxvii GL Song, A Atrens, DH StJohn, J Nairn and Y Lang, Electrochemical Corrosion of Pure Magnesium in 1N NaCl, *Corrosion Science* 39 (1997) 855

xxxviii GL Song, A Atrens, D StJohn, X Wu and J Nairn, Anodic Dissolution of Magnesium in Chloride and Sulphate Solutions, *Corrosion Science* 39 (1997) 1981-2004

xxxix GL Song, A Atrens, X Wu and B Zhang, Corrosion Behaviour of AZ21, AZ501 and AZ91 in Sodium Chloride, *Corrosion Science* 40 (1998) 1769-1791

xl GL Song, A Atrens and M Dargusch, Influence of Microstructure on the corrosion of diecast AZ91D, *Corrosion Science* 41 (1999) 249-273

xli D.A. Jones, "Principles and Prevention of Corrosion", Macmillan Publishing Company, New York, 1992

xlii A. Oehlert, "Primary Creep and Stress Corrosion Cracking in High Strength Steels", PhD Thesis, The University of Queensland, 1994

xliii J.L. Crolet, M.R. Bonis, “Revisiting Hydrogen in Steel, Part 1: Theoretical Aspects of Charging, Stress Cracking and Permeation”, proceedings of *Corrosion 2001*, Houston, NACE, Paper No. 01067

xliv F.M. Al-Faqueer, H.W. Pickering, “Kinetics of Electrochemical Hydrogen Absorption in Metals”, in *Hydrogen Effects on Materials Behavior and Corrosion Deformation Interactions*, N.R. Moody, A.W. Thompson, R.E. Ricker, G.W. Was, R.H. Jones, TMS, 2003, p17-33

xlv A Atrens, JJ Bellina, NF Fiore and RJ Coyle. The Diffusion of Hydrogen in Austenitic Stainless Steels During and After Electrolytic Charging *The Metal Science of Stainless Steels,* WE Collings and HW King, Editors, TMS-AIME, (1978) 54-69.

xlvi A Atrens, D Mezzanotte, NF Fiore and MA Genshaw. Electrochemical Studies of Hydrogen Diffusion and Permeability in Ni, *Corrosion Science* 20 (1980) 673-684.

xlvii F.S. Ham, “Stress Assisted Precipitation on Dislocations”, Journal of Applied Physics, 1959, Vol 30, p915-926

xlviii A. Atrens, N. Winzer, G. Song, W. Dietzel, C. Blawert, “Stress Corrosion Cracking and Hydrogen Diffusion in Magnesium”, *Advanced Engineering Materials*, 8, pp749-751, 2006

xlix M.P. Puls, “The Effects of Misfit and External Stresses on Terminal Solid Solubility in Hydride Forming Metals”, Acta Metallurgica, 1981, Vol 29, pp1961-1968

l F.R.N. Nabarro, “The Strains Produced by Precipitation in Alloys”, Proceedings of the Royal Society of London. Series A, Mathematical and Physical Sciences, Vol. 175, No. 193, 1940, pp519-538

li J.D Eshelby, “The Determination of the Elastic Field of an Ellipsoidal Inclusion and Related Problems”, Proceedings of the Royal Society of London. Series A, Mathematical and Physical Sciences, Vol. 241, No. 1226, 1957, pp376-396

lii J.D Eshelby, “The Determination of the Elastic Field of an Ellipsoidal Inclusion and Related Problems”, Proceedings of the Royal Society of London. Series A, Mathematical and Physical Sciences, Vol. 241, No. 1226, 1957, pp376-396

liii N.F. Mott, F.R.N Nabarro, “An Attempt to Estimate the Degree of Precipitation Hardening, With a Simple Model”, Proc. Phys. Soc., 1940, 52, 86

liv F.H. Ellinger, C.E. Holley, Jr., B.B. McInteer, D. Pavone, R.M. Potter, E. Staritzky, W.H. Zachariasen, “The Preparation and Some Properties of Magnesium Hydride”, J. Am. Chem. Soc., 1955, 77, pp2647-2648

lv R. Yu, P.K. Lam, “Electronic and Structural Properties of MgH2”, Physical Review B, 1988, Vol 37, 15, pp8730-8738

lvi http://www.matweb.com/search/SpecificMaterial.asp?bassnum=MMAZ96

lvii C Nishimura, M Komaki and M Amano, Hydrogen permeation through magnesium, *Journal of Alloys and Compounds* 293-295 (1999) 329-333.

lviii JF Stampfer Jr, CE Holley Jr, JF Suttle, The Magnesium-Hydrogen System, *Journal of the American Chemical Society*, 82 (1959) 3504.

lix A Krozer and B Kasemo, Equilibrium hydrogen uptake and associated kinetics for the Mg-H2 system at low pressures, *Journal of Physics: Condensed Matter,* 1 (1989) 1533.

lx AS Ingason and S Olafsson, Thermodynamics of hydrogen uptake in Mg films studied by resistance measurements, *Journal of Alloys and Compounds,* 404-406 (2005) 469-472.

lxi MA Avedesian and H Baker Eds Magnesium and magnesium Alloys, ASM International, Materials Park, Ohio USA (1999).

lxii CD Cann and A Atrens. A Metallographic Study of the Terminal Solubility of Hydrogen in Zirconium at Low Hydrogen Concentrations, *J. Nuclear Materials*, 88 (1980) 42-50.

lxiii S.Q. Shi, M.P. Puls, "Criteria for Fracture Initiation at Hydrides in Zirconium Alloys I. Sharp Crack Tip", Journal of Nuclear Materials, 1994, 208, pp232-242

lxiv S.Q. Shi, M.P. Puls, S. Sagat, "Criteria for Fracture Initiation at Hydrides in Zirconium Alloys II. Shallow Notch", Journal of Nuclear Materials, 1994, 208, pp243-250

lxv M. Stioui, A. Grayevski, R. Resnik, D Shaltiel, N. Kaplan, "Macroscopic and Microscopic Kinetics of Hydrogen in Magnesium-Rich Compounds", *Journal of the Less-Common Metals*, 1986, 123, pp9-24

lxvi M Pfuff, GKSS, private communication Jan 2007

Figure(s)

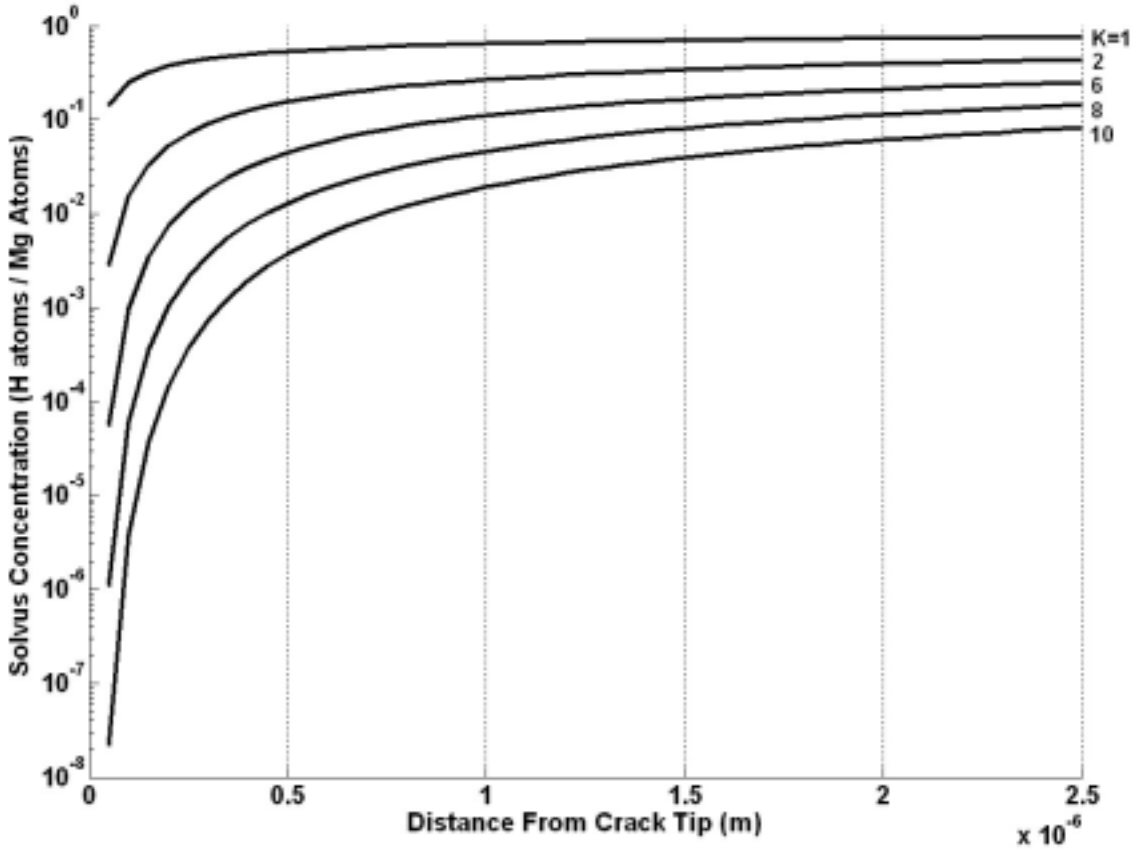

Figure 1 – Normalised concentration c_s^{σ}/c_{con} for various stress intensities (in MPa.m$^{1/2}$) in the region ahead of the crack tip.

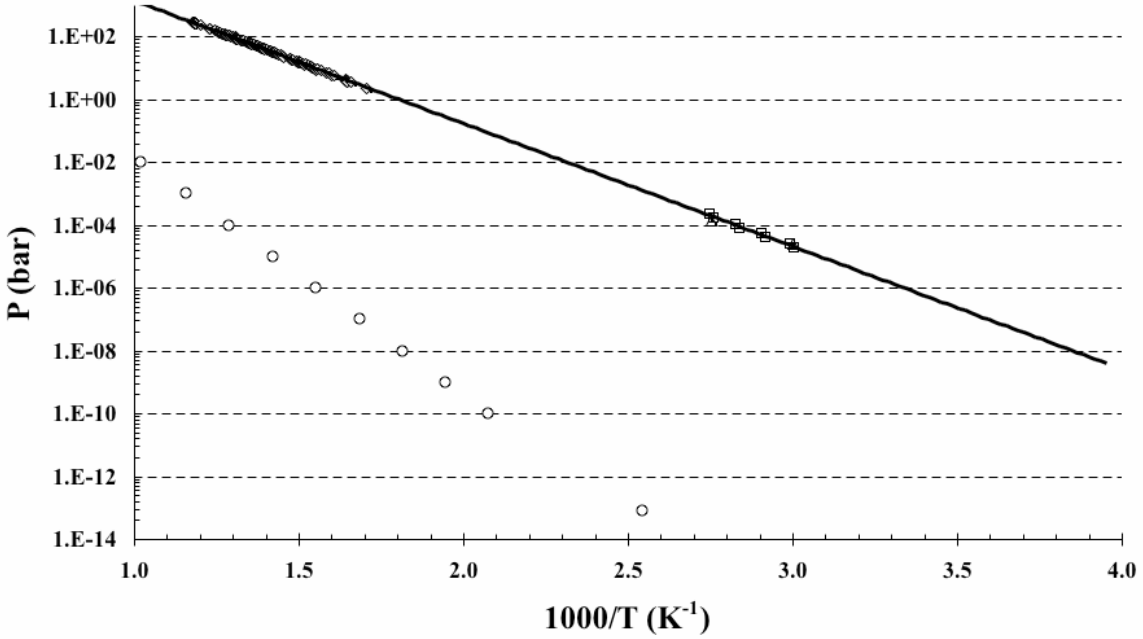

Figure 2 – Solvus concentration as *P*(H) of H in Mg & Mg vapour pressure (○).

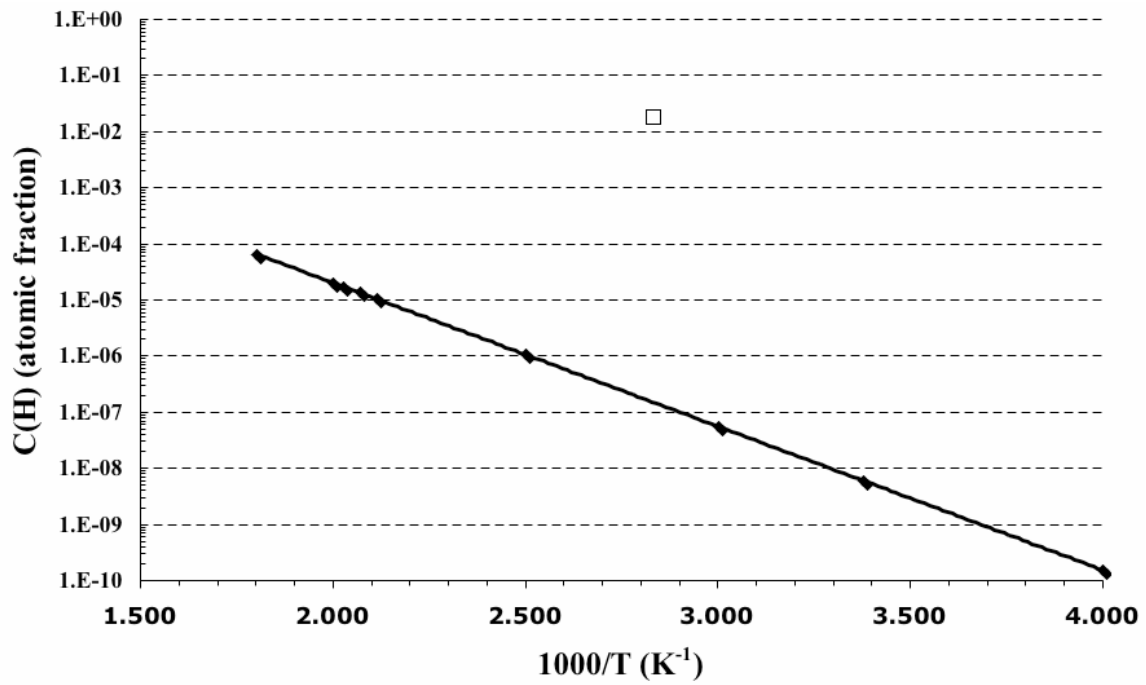

Figure 3 – Solvus concentration (as an atomic fraction) for H in Mg in the temperature range -23 to 282C compared with data point of Krozer and Kasemo (□).

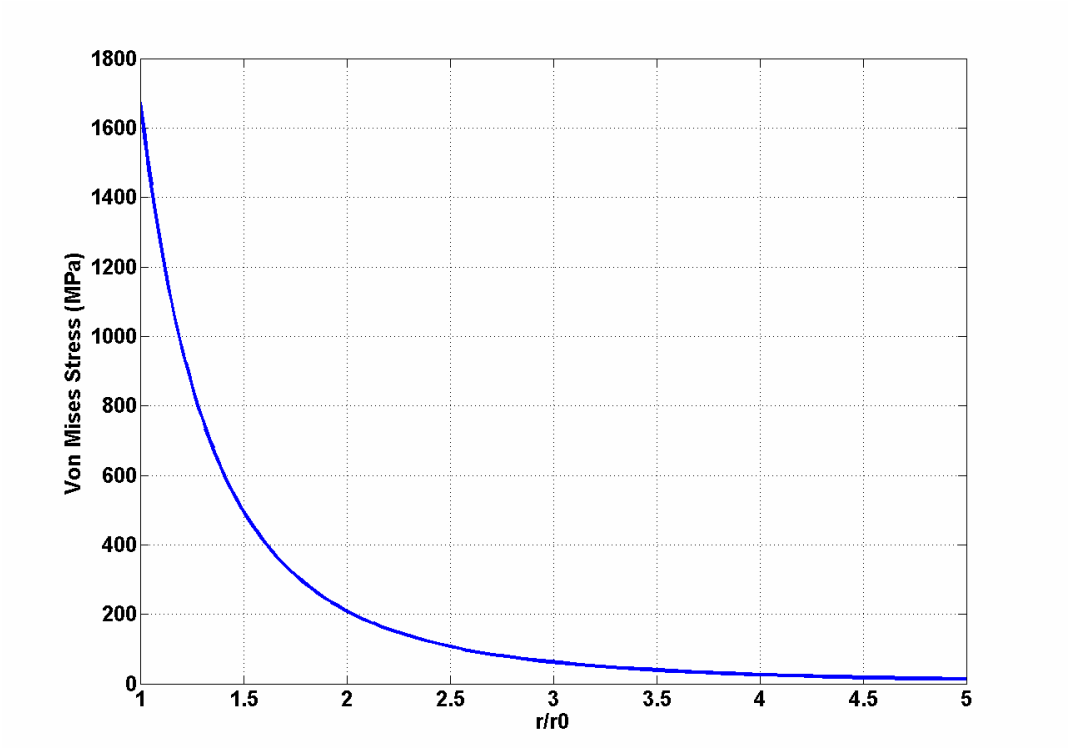

Figure 4 - Accommodation stress for a spherical hydride.

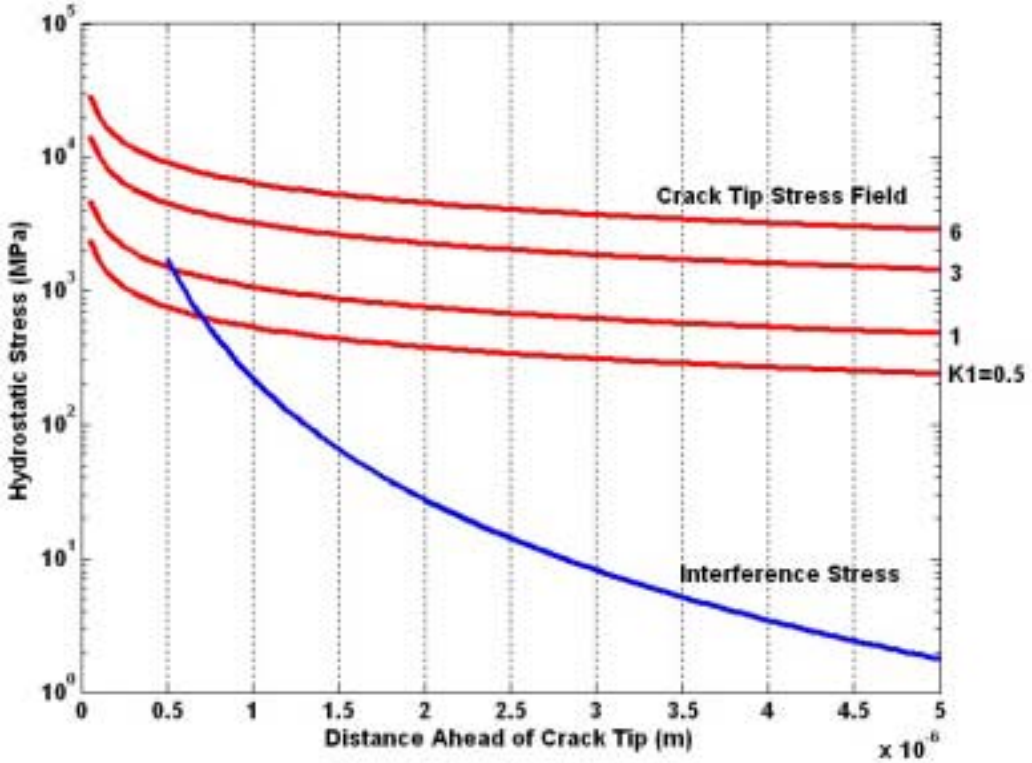

Figure 5 - Comparison between absolute values for the crack tip stress field for various stress intensities (in MPa.m$^{1/2}$) and the stress due to the volumetric misfit for a spherical hydride of radius 0.5 μm.

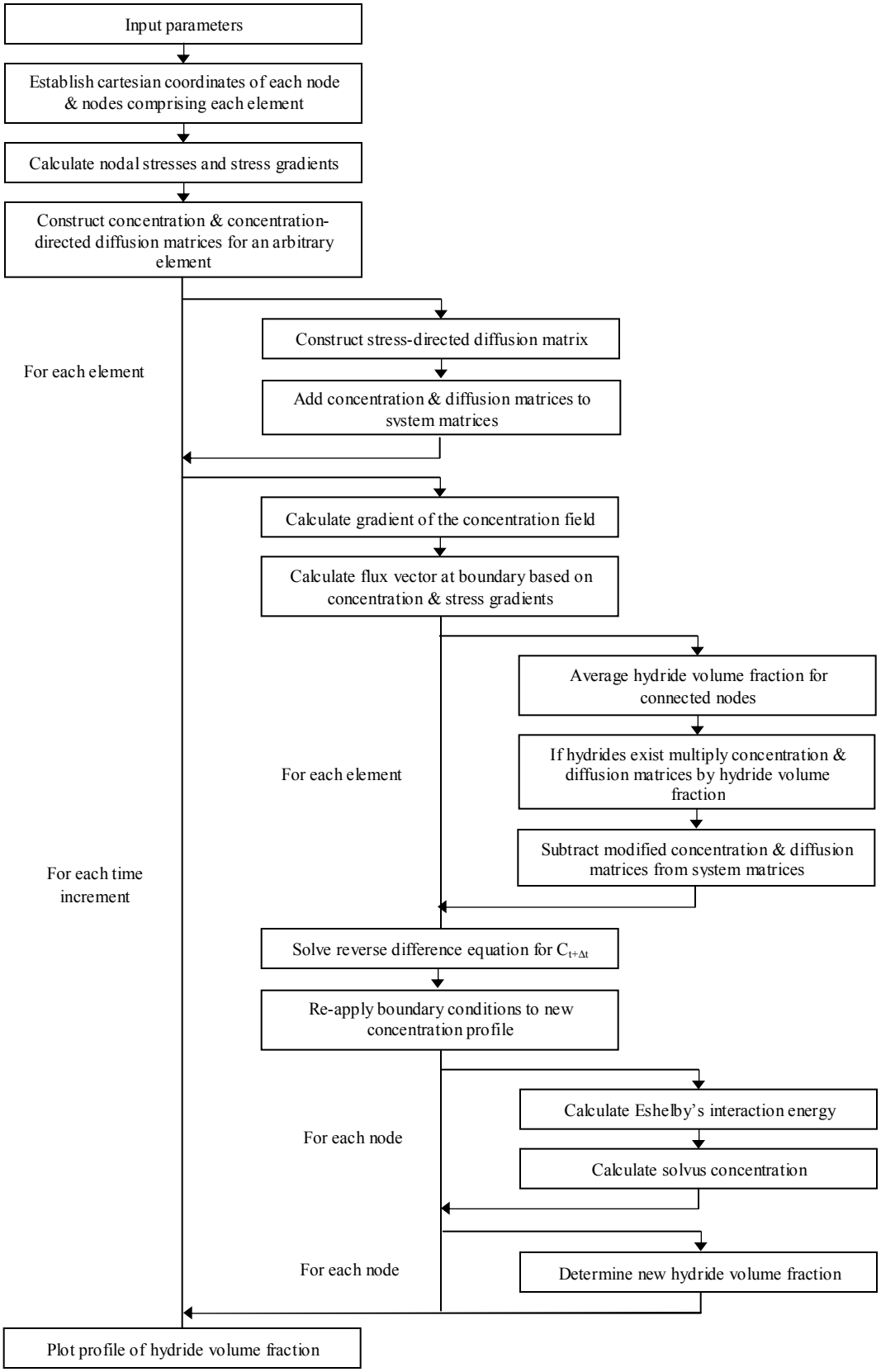

Figure 6 – Flow diagram for finite element program logic.

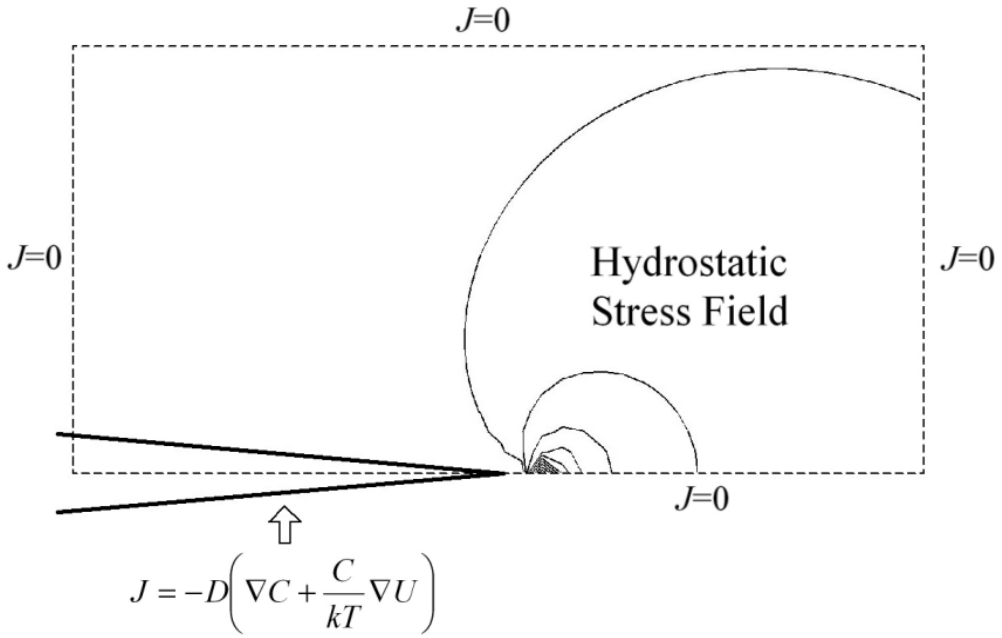

Figure 7 – Boundary conditions for finite element formulation of hydride formation ahead of a sharp crack tip.

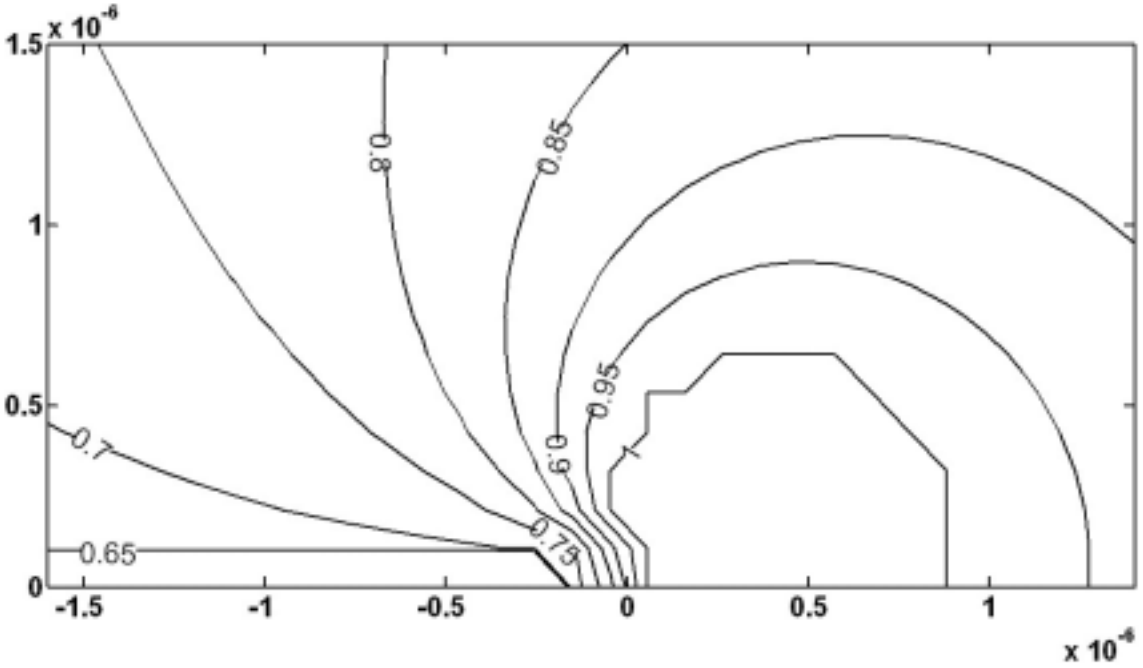

Figure 8 – Distribution of the hydride volume fraction f for $K_1 = 6$ MPa.m$^{1/2}$ and $t = 6.2$ sec.

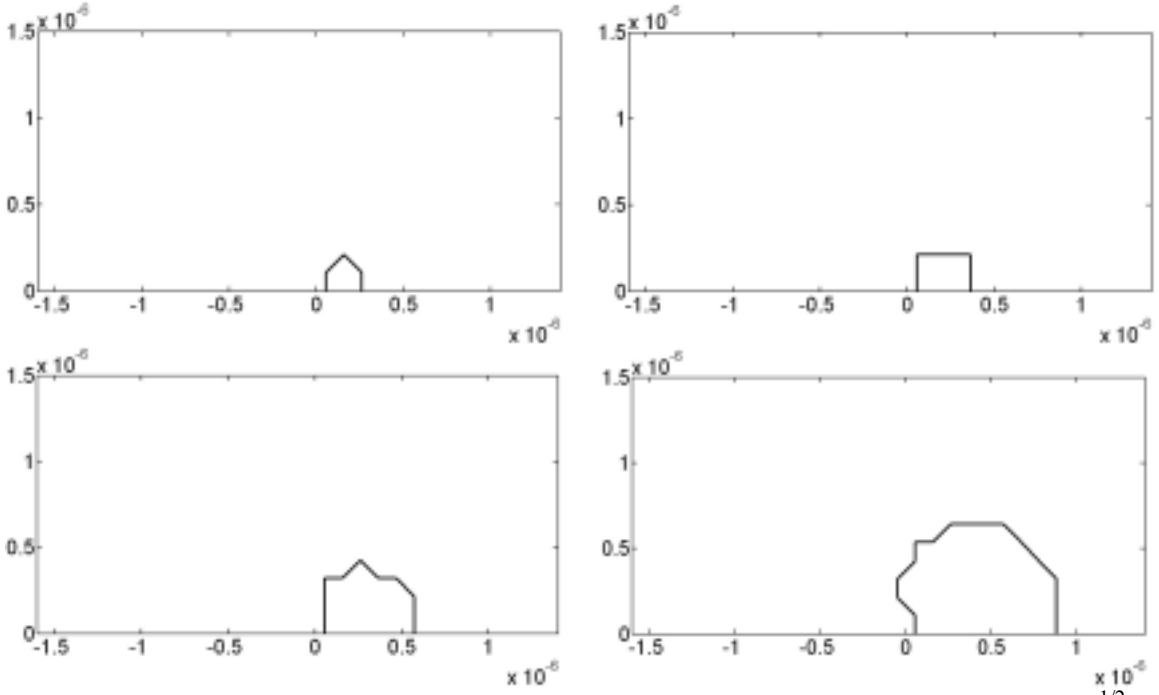

Figure 9 – $f = 1$ zone after 6.19 sec, 6.2 sec, 6.21 sec and 6.22 sec for $K_1 = 6$ MPa.m$^{1/2}$.

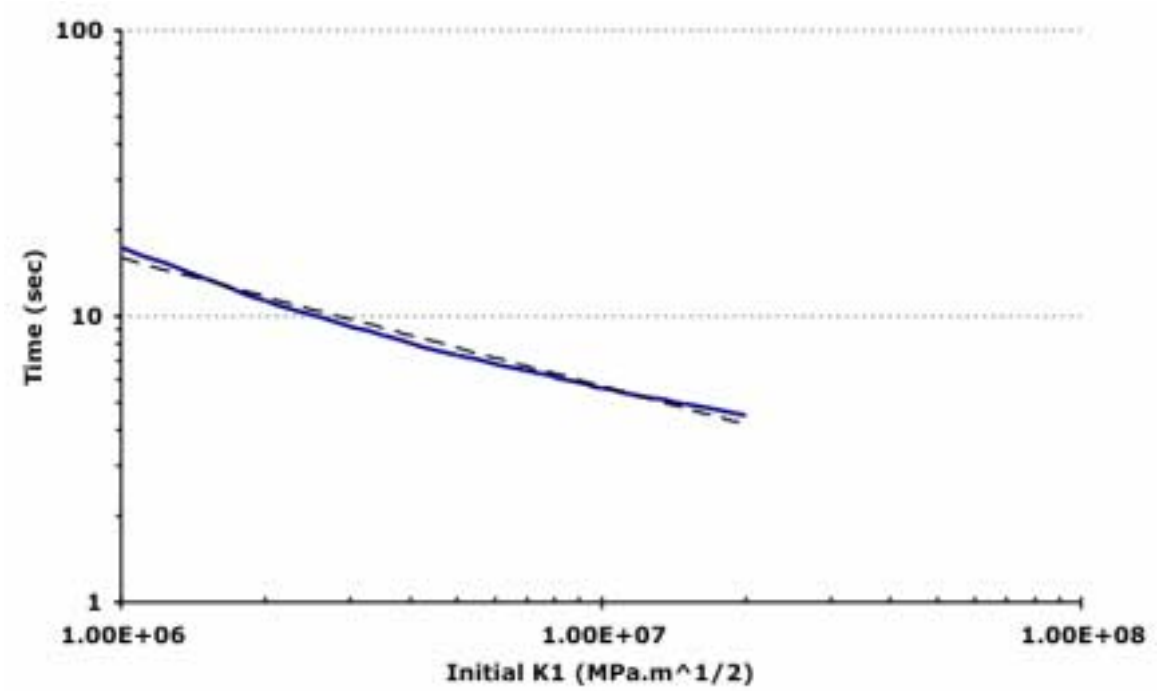

Figure 10 – The influence of K_1 near K_{1SCC} on the time required for the $f = 1$ hydride front to reach a distance of ~0.8 μm ahead of the crack tip.

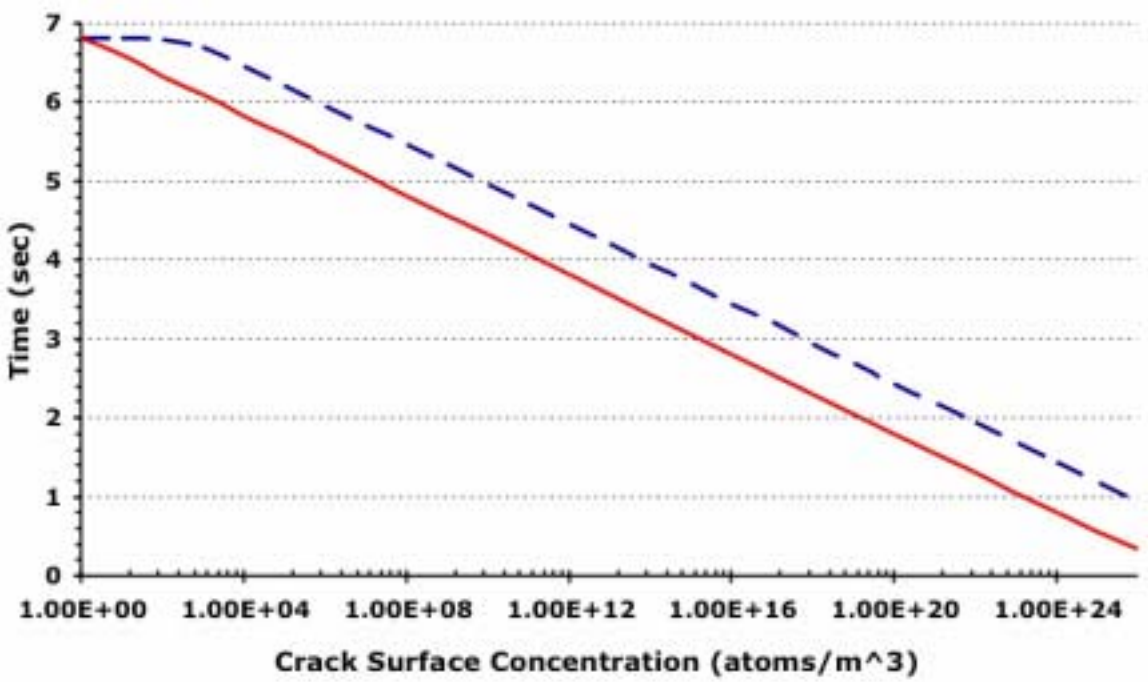

Figure 11 – The influence of the crack surface H concentration, C_{surf}, on the time to reach the critical hydride size, t, for $K_1 = 6$ MPa.m$^{1/2}$. The dashed line shows the influence of C_{surf} on t when the flux through the crack surface is dependent on the stress gradient only